

Fluid transport by solitary waves along growing faults A field example from the South Eugene Island Basin, Gulf of Mexico

A. Revil^{a,*}, L.M. Cathles III^b

^a CNRS–CEREGE, Department of Hydrogeophysics and Porous Media, BP 80, 13545 Aix-en-Provence Cedex 4, France

^b Cornell University, Snee Hall, Department of Geological Sciences, Global Basin Research Network, Ithaca, NY 14853, USA

Received 18 November 2001; received in revised form 10 June 2002; accepted 19 June 2002

Abstract

The Red Fault system is one of the main growth faults found in the South Eugene Island Basin, a salt withdrawal minibasin located offshore Louisiana, in the Gulf of Mexico. This fault system corresponds to a lateral boundary between fluid overpressured compartments. In addition, there is a set of observations indicating that the Red Fault system exhibits rapid episodic migration of fluids. This fault represents an example of preferential pathway for the upward episodic migration of overpressured hydrocarbons from deep, heavily pressured, compartments on time scales of years. The migrations of fluids into active growing faults could take the form of propagating surges (solitary waves) that propagate upward along the fault planes in a wave-like manner at km/yr. Solitary waves represent a very efficient mechanism for the upward transport of fluids along growth faults in sedimentary basins generating its own permeability. In addition, this mechanism is compatible with the fact that the fault plane is observed to sustain a static pore fluid pressure difference between its two sides. The propagation of solitary waves in active growth faults appears as a fundamental mechanism to understand the nature of upward fast migration of fluids along active growth faults in compartmentalized sedimentary basins. © 2002 Elsevier Science B.V. All rights reserved.

Keywords: faults; permeability; compaction; plastic deformation

1. Introduction

Siliciclastic-filled sedimentary basins, like found in the Gulf Coast of Mexico, exhibit very often abnormal fluid pressures, i.e. fluid pressures above hydrostatic levels. This phenomenon is clearly related to the presence of sealing mechanisms,

which impede or at least slow down groundwater flow resulting from compaction of the sedimentary column and sedimentation at its top. Such sealing mechanisms are for example related to the presence of low-permeability formations, like smectite-rich shales and evaporite rocks [1], and/or capillary blockage phenomena in presence of a gas-phase and an alternation of sand/shales formations [2]. Ortoleva and various other authors [3] have suggested in the last decade the concept of ‘pressure compartmentation’ in these basins whereby seals prevent or reduce groundwater

* Corresponding author. Tel.: +33-4-4297-1551;
Fax: +33-4-4297-1559.
E-mail address: revil@cerege.fr (A. Revil).

flow at geological time scales. In such a compartmentalized system, the role of growth faults as preferential fluid flow pathways is still poorly understood. Faults are sometimes described as lateral impermeable boundaries or preferential fluid flow pathways [4].

Since 1972, over 270 million barrels of oil and 4×10^{-2} trillion cubic meters of gas (mainly methane) have been produced from the South Eugene Island (SEI) Minibasin, Gulf Coast of Mexico, offshore Louisiana (Fig. 1). This makes this basin one of the largest hydrocarbons producing fields in the Gulf of Mexico and in Plio–Pleistocene sediments. This minibasin is also one of the best known due to the vast number of data recorded during more than 30 years of exploration and production [5–8]. The hydrocarbons contained in all the Late Pliocene and Pleistocene siliciclastic formations (2.20–0.01 Ma) show abundant evidence of long-distance vertical migration over a very short period of time (~ 0.5 My) [7,9,10]. So far, no conclusive answer has been found to explain how these enormous amounts of oil and gas were able to fill the sand reservoirs of this minibasin in this time frame. A similar problem arises in accretionary prisms where numerous observations show that low-angle mud-rich faults can channel huge amounts of fluids from deeply buried source regions. Clearly, the ascent of over-pressured fluids along fault planes is still a poorly understood process and there must be a mechanism that transforms fault zones into regions of transiently highly focused flow. Various authors [11–13] have already emphasized the role of faults in episodic fluid expulsions in sedimentary basins. We discuss here the possibility that fluids are transiently channelled along the fault plane through the propagation of solitary waves, which constitute a very efficient mechanism for rapid fluid transfer through the sedimentary column. We will focus our discussion on the role of the main

active growth fault system located into the SEI area, called the Red Fault system (see Figs. 1 and 2), as a preferential pathway for the upward migrations of fluids in this basin.

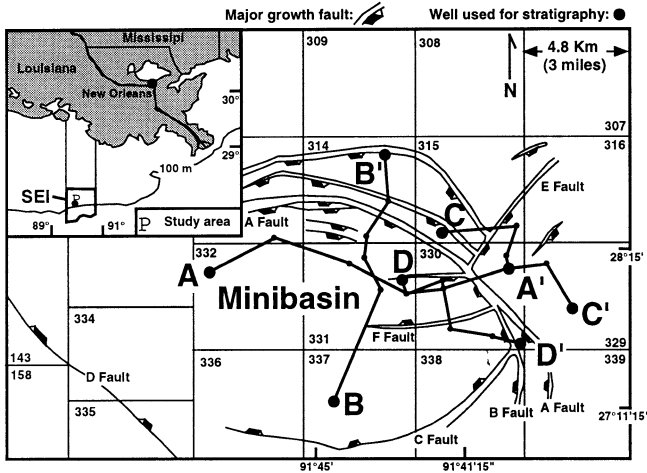
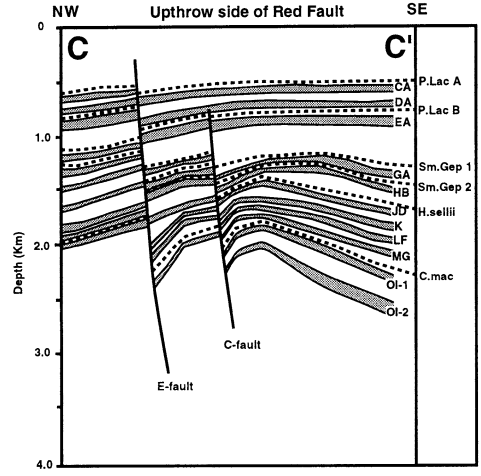
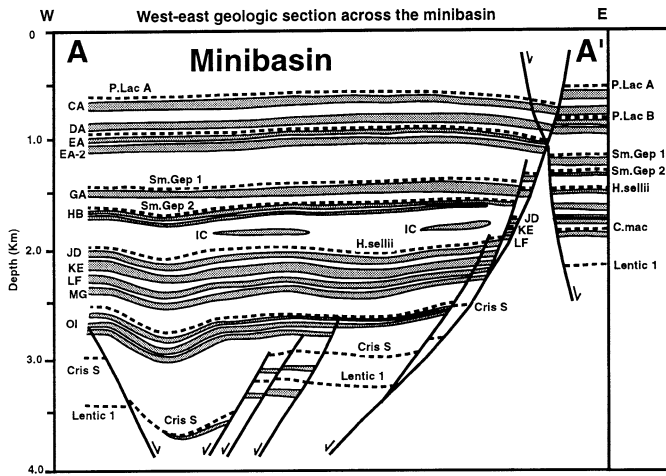
2. The Red Fault system

In November and December of 1993, a joint project between the Global Basin Research Network (GBRN), a consortium of universities and industry affiliates, the American Department of Energy, and private oil industry led to drilling a test well, called the Pathfinder Well, through the Red Fault system (Figs. 1 and 2). The purpose of this project was to bring some answers to the question of the rapid fluids migration (especially oil and gas) in this basin. We summarize in this section the main results found during this drilling and other drillings operated by the oil industry in this area and we make a synthesis of observations already published and related to this project. This sum of observations will be used in Section 3 to propose a new transport mechanism by solitary waves (pressure pulses) propagating along the fault planes.

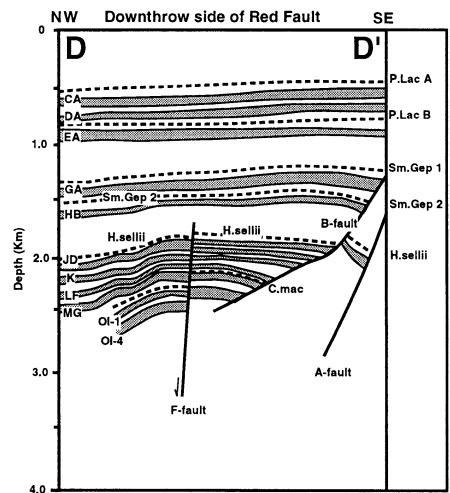
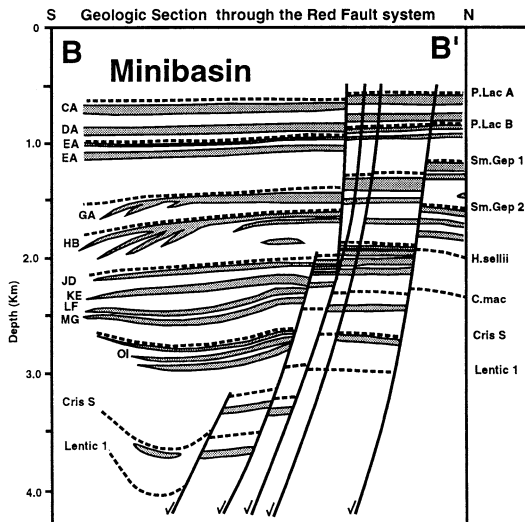
2.1. Fluid pressure, effective stress, and mechanical properties

Seismic sections, log data, and petrophysical measurements were carried out in the purpose to understand both compartmentation and the role of the Red Fault in the hydrodynamics of the minibasin [14]. Among this vast amount of data, those reported in Fig. 3 show that the Red Fault system acts as a lateral permeability barrier supporting 5–10 MPa of pore fluid overpressure between the two compartments observed on both sides. The effective stress measured in the Red Fault system itself is very low, only few MPa

Fig. 1. Location map and cross-section based on downhole measurements and seismic interpretation showing the main sand formations in the SEI minibasin. The main sand formations are grey-shaded and the surfaces the geological age of which are known are drawn as black dashed lines. The bio-stratigraphic information is given to provide the age of the formations and an idea of the extremely high sedimentation rate in this area (> 2 km per My). The stratigraphic cross-sections are modified from Alexander and Flemings [5] and Coelho [6]. The faults shown on the location map are represented from the seismic data at a depth of ~ 2 km.



Fossil zones	Age in Ma (Max.,Min.)	Paleobathymetry (m)
P.Lac.A	0.46 (0.51-0.46)	15
P.Lac.B	0.65 (0.75-0.46)	37
Sm.Gep.1	0.9 (0.9-0.9)	91
Sm.Gep.2	1.2 (1.2-1.2)	91
H.Sellii	1.27 (1.35-1.19)	100
C.Mac	1.50 (1.54-1.5)	91
Lentic 1	2.2 (2.25-2.15)	100



South Eugene Island (SEI)
Minibasin

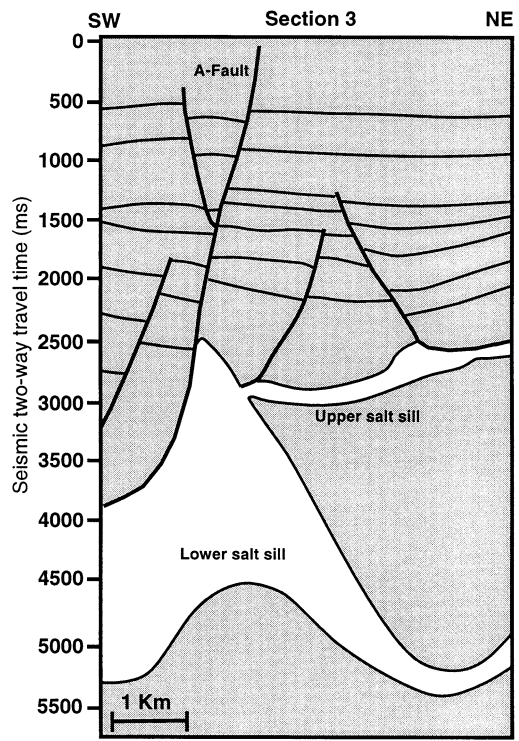
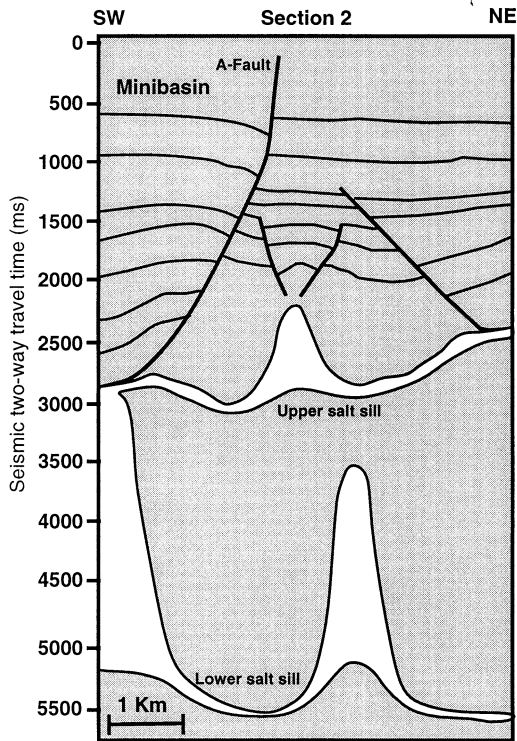
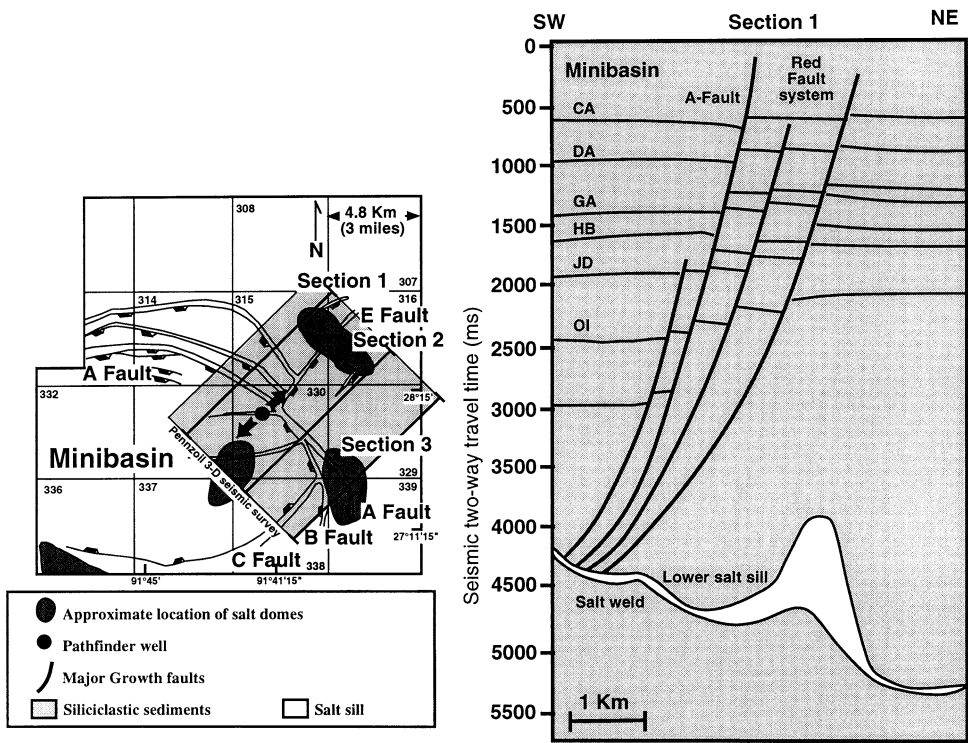


(Fig. 4), indicating that the system itself is over-pressured. In addition, downhole measurements in the Red Fault system and core measurements [15] indicate that the material found in the fault zone is mechanically very weak, with a high undrained Poisson's ratio (~ 0.40 – 0.45) and a low shear modulus (~ 1.1 – 1.4 GPa). Therefore the fault gouge behaves similarly to a viscous fluid (high Poisson's ratio), and the deviatoric stress in the fault zone remains probably very low during its activity. Consequently, the Red Fault is weak in a relative sense, as the surrounding sediments seem mechanically stronger. The fact that the Red Fault is still active today, whereas most of the salt withdrawal from the minibasin depocenter is accomplished, implies that the Red Fault is also weak in an absolute sense, i.e. the fault can move under small differential loading stresses. Pevska and Zoback [16] investigated the occurrence of compressive and tensile failures in the Pathfinder Well. They showed that the minimum horizontal principal direction is nearly 90° to the trace of the Red Fault, an angle much larger than predicted from standard frictional failure considerations. This reinforces the fact that the Red Fault is weak in an absolute sense.

2.2. Permeability and porosity

The dependence of the permeability upon the effective stress in the Red Fault system has been the subject of in situ measurements just after the completion of the Pathfinder Well. It was found that the permeability of the fault gouge material is a strongly decreasing function of effective stress (Fig. 5), and hence a strongly increasing function of the pore fluid pressure. In situ measurements are well represented by the permeability/effective stress relationship suggested by Rice [17]:

$$k = k_0 \exp(-\sigma_{\text{eff}}/\sigma^*) \quad (1)$$

where σ_{eff} is the effective stress ($\sigma_{\text{eff}} = (\sigma - p)$ where σ is the confining pressure, approximated by the lithostatic stress, and p is the pore fluid pressure), k_0 is the permeability at zero effective stress, and σ^* is a constant, which characterizes the influence of the compactional response of the porous material upon the permeability. The data displayed in Fig. 5a correspond to drill stem data from the Pathfinder Well in a perforated and fracture-packed interval from 2185 to 2198 m true vertical depth around the A-fault (see Fig. 1). The use of Eq. 1 and the drill stem data of Fig. 5a yield $k_0 = 668$ mD and $\sigma^* = 0.25$ MPa. Such a low value of σ^* corresponds usually to highly cracked rocks [17]. This is consistent with the fact that a high density of cracks and fractures were observed in the soft fault gouge materials cored during the drilling of the Pathfinder Well [7]. The matrix permeability of the silty shale is in the range 10–01 microdarcy in the effective stress range 01–10 MPa [18], so much below the value of the fractured shale. The measurements performed by Elliott [18] are done on small cores, which do not sample the macrocracks previously discussed. This is a classical scaling problem, which implies that the permeability measurements obtained by Elliott [18] are characteristic of the background (matrix) permeability, which is much smaller than the fractured shale permeability of the gouge.

The model developed in Section 3 will require the value of the compaction coefficient. Elliott [18] has performed consolidation tests using core samples from the Pathfinder Well. One of these tests is shown in Fig. 5b. These data represent porosity versus effective stress under conditions where the effective stress increases monotonically and then decrease monotonically (only data above few MPa are shown, the maximum previous consolidation stress was estimated by Elliott to be 7 MPa). For both normal consolidation and elastic

←

Fig. 2. Location and interpretation of three seismic sections taken from the 3-D Pennzoil seismic data cube (modified from Coelho [6]). These sections show selected sand formations, growing faults, and the salt sills. Note that the geometry of the base of the salt sill follows more or less the geometry of the top due to a pull effect caused by the high seismic velocity in the salt. Section 1 shows that the Red Fault system soles out over a salt weld in the lower salt sill, which could provide a pathway for upward migration of fluids from deep compartments located below the lower salt sill. Sections 2 and 3 show evidence of an upper salt sill adjacent to the SEI minibasin. A second system of growing faults seems to stop at the upper salt sill.

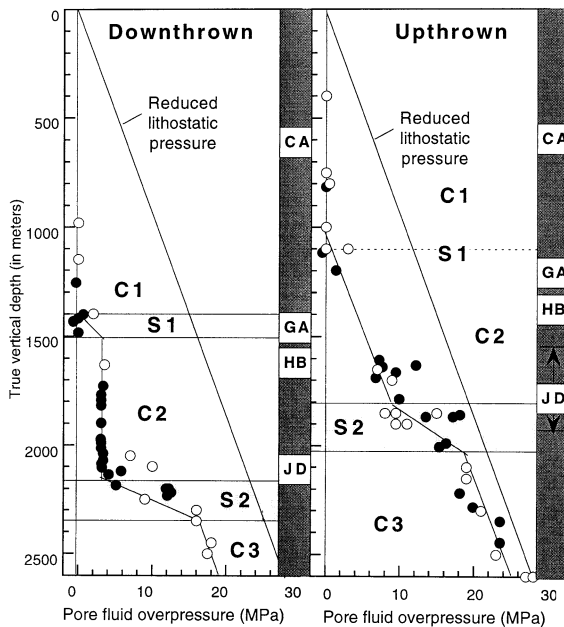


Fig. 3. Pore fluid overpressures (in MPa) in the downthrow and upthrow sides of the Red Fault system (Block 330). Three compartments can be observed on each side: C1 is the hydrostatic upper portion of the basin, C2 is a softly pressurized compartment, and C3 is a highly pressurized compartment. The boundaries S1 and S2 correspond to permeability barriers (shale and/or capillary barriers). Note the correlation between the location of S2 and the presence of the JD sand (the arrows surrounding the location of the JD sand on the upthrow side correspond to the shallowest and deepest depth of location of this sand). The filled circles correspond to direct pressure measurements made in the boreholes. The open circles represent mud weight data. The mud weight data correspond to the weight of the drilling mud used to drill the borehole and adjusted to compensate the fluid pressure of the formations in order to avoid any blow out of the borehole.

swelling from a pre-consolidated state, the porosity is linearly related to the effective stress for the effective stress range considered in Fig. 5b. The compressibility for elastic swelling ($\beta \approx 1.0 \times 10^{-8}/\text{Pa}$) is roughly three times smaller than the compressibility associated with 'normal' consolidation ($\beta \approx 2.7 \times 10^{-8}/\text{Pa}$).

2.3. Geochemical anomalies

Geochemical evidence from core samples taken

from boreholes intersecting the Red Fault system and from the shallow reservoirs drilled in the SEI minibasin [6–8,10,19,20] indicates that (1) the oil sampled from shallow (< 1 km) 0.5-Ma-old reservoirs is a 50–90-Ma-old oil that had spent most of its life at depths greater than 6 km; (2) the oil source rock is a deep Mesozoic carbonate (depth ~9–14 km); (3) the geochemical signature of the oil filling the open fractures observed in the Red Fault system is similar to that found in the shallow sandy reservoirs; and (4) hydrocarbons make their journey from about 6 km up to the shallow sand reservoirs in just a couple of years [20]. Sediments collected at the seafloor of the SEI area, along the trace of the Red Fault system, exhibit hydrocarbon micro-seepages, which suggest present-day fluid migration associated with this major growth fault system [9].

2.4. Temperature anomaly

A positive temperature anomaly of about 10°C is associated with the Red Fault system in both footwall and hanging walls [9] and paleothermal anomalies based on vitrinite reflectance have also been reported in some sections of the Red Fault [8]. Using a 3-D dynamic finite-element model, Coelho [6] showed that the thermal anomaly observed in SEI area Block 330 is probably a combination of rapid venting through the Red Fault system combined with lower thermal conductivity (and thus higher geothermal gradient) caused by the presence of trapped oil and gas on the hanging wall of the Red Fault. Indeed gas and oil in the pores have a strong influence upon the effective thermal conductivity of granular sediments [21]. Geochemical indicators of mass and heat flux show that the Red Fault system has acted as a conduit for ascending hot fluids [8]. Losh et al. [8] concluded that 'simple modelling of coupled heat and mass flux indicates the paleothermal anomaly (...) was short-lived, having a duration less than 150 years. The anomaly could have been produced by a $2 \times 10^6 \text{ m}^3$ pulse of fluid ascending the fault at an actual velocity of over 1 km/yr from 3 km deeper in the basin'. However, no mechanism was proposed to explain such a

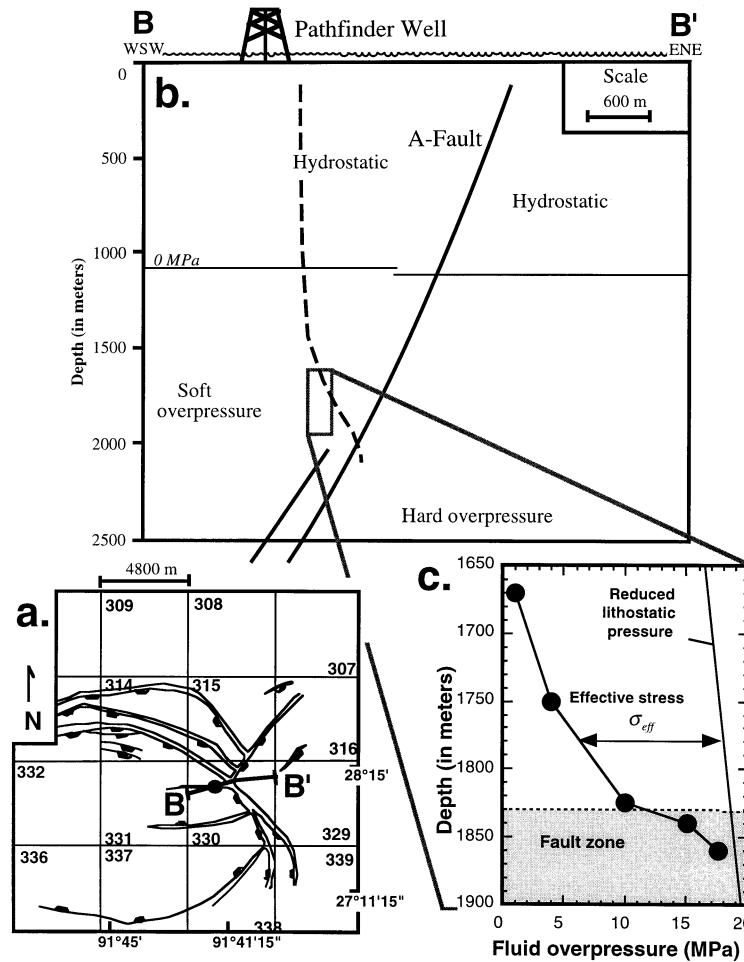


Fig. 4. (a,b) Location of the Pathfinder Well. (c) Fluid pressure in excess of hydrostatic in the Pathfinder Well. Note the low effective stress in the fault zone.

rapid venting phenomenon. Such a mechanism will be proposed in Section 3.

2.5. Seismic anomaly

Anderson et al. [10] analyzed repeated 3-D seismic section obtained in the SEI minibasin. They observed ‘trails’ of high seismic amplitudes leading from the shallow reservoir to the Red Fault system, and then to deep turbiditic sands extending deep within the hard pressures. They proposed that these trails could be associated with hydrocarbon migration pathways and high fluid pressure above hydrostatic.

2.6. The role of salt sills

The upper sedimentary portion of the basin is mechanically decoupled from the lower section (say below 6 km depth) by the weak salt sills. Viscous flow of the salt sills is responsible of salt welds, i.e. regions where all the salt has evacuated. A salt weld represents a leakage point for pressured fluids to move up from the deep overpressured formations located below the salt sill. Thus, there may be an inherent coupling between the viscous flow of salt forming salt domes, which requires growth faulting in the overlying sedimentary piles, and the supply of fluid pressures from

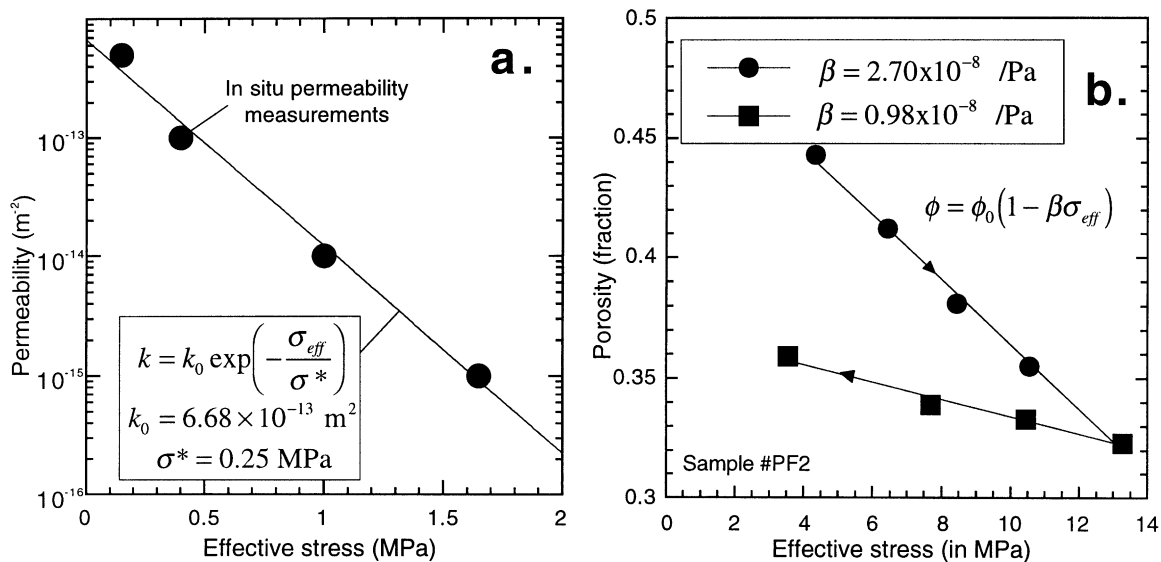


Fig. 5. Permeability and porosity versus effective stress. (a) Direct in situ permeability measurements inside the Red Fault system. These data can be fitted by an exponential law where k_0 is the permeability at zero effective stress and σ^* is a pressure sensitivity constant for permeability. (b) Laboratory measurements of normal compaction and elastic swelling of a shale core from the SEI area (data from [18]). Pore water: 2 M NaCl brine.

deep compartments, which allows faulting to take place at low effective stresses. The high fluid pressures (probably approaching lithostatic) in the compartments located below the salt sills are probably due to various phenomena including maturation of the kerogen and disequilibrium compaction as indeed the continuous portion of the salt sills is impermeable to groundwater flow.

Based on stratigraphic evidence, Alexander and Flemings [5] showed that the Red Fault system experienced its highest slip rate during deposition of the deltaic sand–mudstone sequence ~ 1.8 – 1.0 Ma ago. Current activity of the Red Fault system is implied by its presence at the shallowest resolvable depths in seismic data [7]. Hanging-wall deformation and stress analysis [7,16] are consistent with normal faulting.

From the previous set of observations, the following picture seems to emerge. Hydrocarbons, generated in a depth range 9–14 km in Mesozoic carbonate formations, spend most of their lives at depths of 5–8 km beneath the salt sills shown in Fig. 2, in highly pressured compartments and at temperatures ~ 110 – 150°C . Note that under these

conditions, oil and gas form a ‘super-critical’ fluid mixture and not separate phases. The fluid pressure in these deep compartments, below the regional salt sills, cannot build indefinitely and hydrofracturation occurs when the fluid pressure reaches the minimum principal stress. When this happens, the oil/gas super-critical mixture forms high-porosity pockets with a high fluid content, which move upward quickly (> 1 km/yr) using salt welds and growing faults as preferential pathways. Then, at some depths, the super-critical oil/gas fluid reaches its bubble point, causing both phases to separate. The pore fluid pressure, temperature, and initial composition of the fluid determine the depth of this phase separation, which probably occurs in the range 2–3 km (Peter Meulbroek, pers. commun., 1998). When they reach the upper section of the growth faults, hydrocarbons (and saline water from the salt sills) can either fill the shallow sandy formations or they can form hydrocarbon seepage at the seafloor. A mechanism of upward fluid transport along fault, which is compatible with all the information available, is envisioned in Section 3.

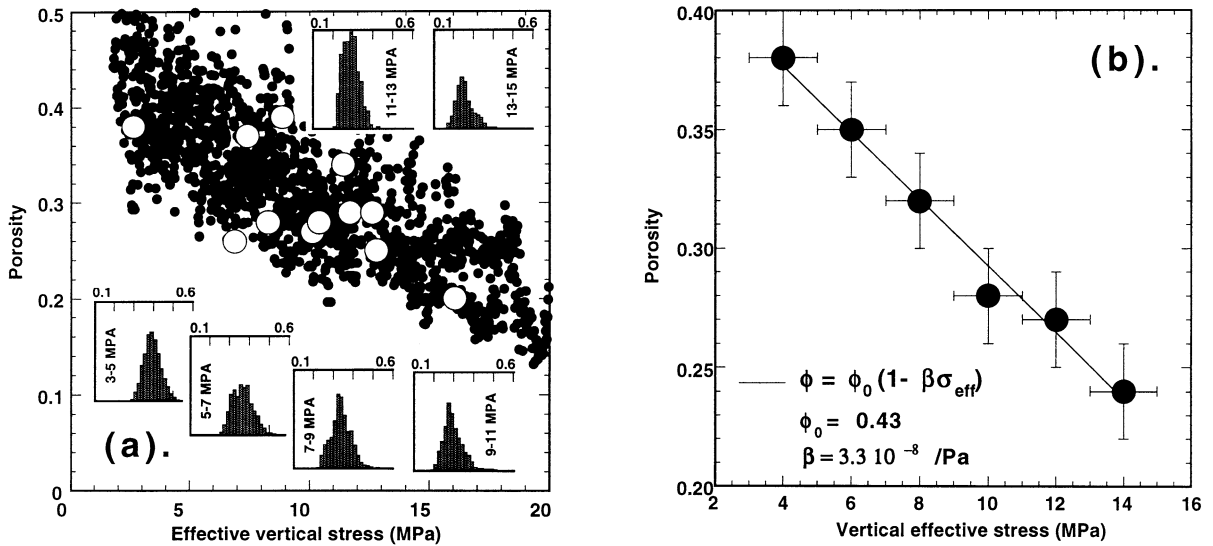


Fig. 6. Porosity versus effective stress. (a) Data from five wells with an average clay content approximately of 60%, and varying locally from 15 (sands) to 80% (shales). Filled circles represent porosity measured by downhole density logs. These measurements report one data point every foot. Only 5% of the points (randomly chosen) are plotted here for clarity. Filled circles represent only data from hydrostatically pressured formations. Open circles represent porosity determined from density measurements in sediments in which pore pressures are greater than hydrostatic and where mud weight data have been used to estimate effective stress. The important scatter of the data is due to the fact that porosity is a function of both lithology and effective stress. The histogram plots represent the porosity distribution (100% of the data used) for the effective stress intervals indicated. (b) Porosity as a function of the effective stress using the maxima of the porosity histogram distributions shown in Fig. 3a. These data show that porosity is linearly related to effective stress with an average non-compacted porosity equal to 0.43, and an average pore compressibility equal to $(3.3 \pm 0.3) \times 10^{-8} \text{ Pa}^{-1}$, which represent values for a sedimentary column of average lithology.

2.7. Compaction trends

In Fig. 6, we report porosity/effective stress data determined from downhole measurement analysis in several boreholes. Fig. 6a shows a lot of scatter in these data due to the influence of lithological variations, especially due to variations with depth in the clay content, upon the porosity. However, when averaged with a sliding window to remove the impact of the lithological variations, a clear linear trend appears between the porosity and the effective stress. This trend is characteristic of compaction. It is used to determine the uncompacted porosity ϕ_0 and the compaction coefficient $\beta \approx 3.3 \times 10^{-8} / \text{Pa}$. Note that the field value of β for the compaction coefficient is remarkably close to the experimental value determined in Section 2.2 from the data obtained by Elliott [18] ($\beta \approx 2.7 \times 10^{-8} / \text{Pa}$, see Fig. 5b). In Fig. 7, we have plotted the porosity and fluid pressure

trends vs. depth for a borehole located on the upthrow side of the Red Fault system. There is a clear link between fluid overpressure and undercompaction in this borehole. Note the existence of a seal inside the sedimentary column, which maintains high fluid pressure levels associated with undercompaction of the sediment below 2000 m (true vertical depth). The occurrence of such a seal could be associated with capillary blockage as suggested in [2].

3. Faults as preferential pathways

A model of growth fault dynamics and fluid migration using the growth faults as preferential pathways should explain the observations reported in Section 2. These observations include (1) the geochemical anomalies of the hydrocarbons showing a high upward migration velocity

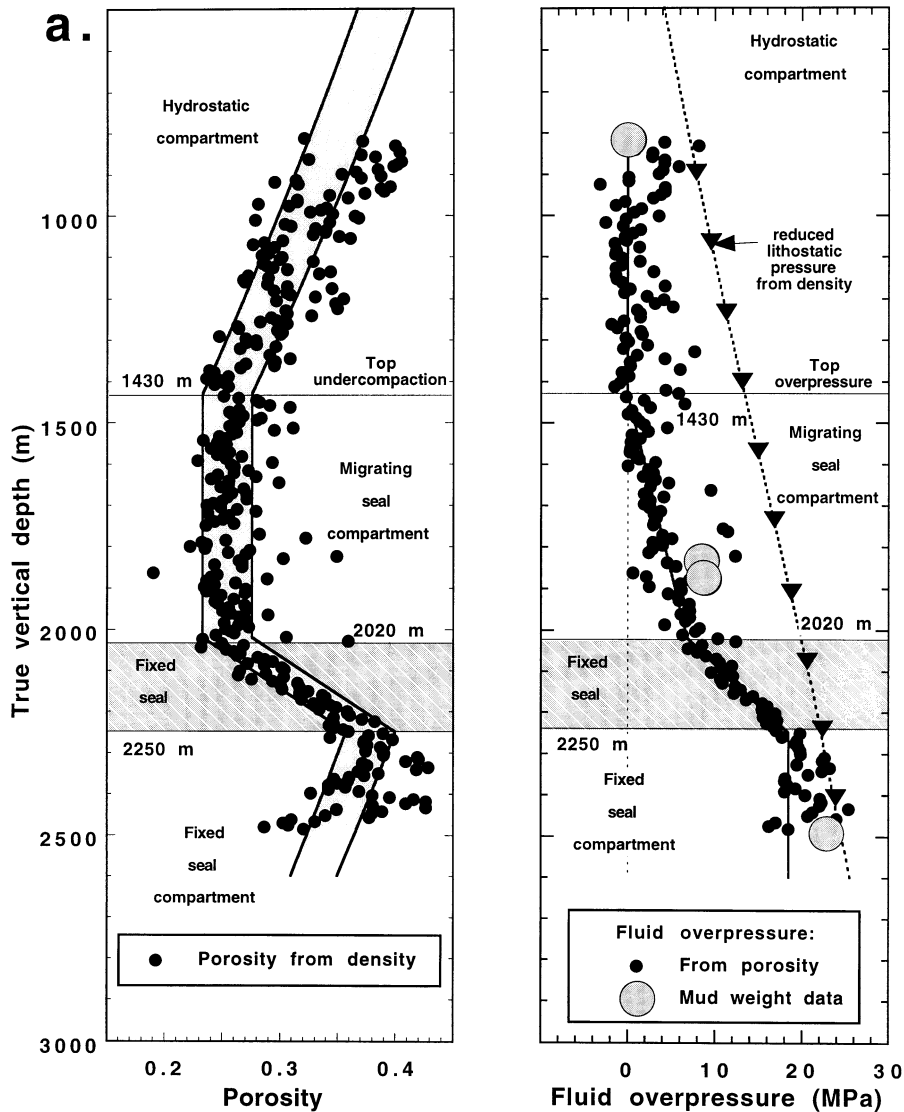


Fig. 7. Example of the porosity and fluid pressure profiles in the upthrow side of the Red Fault. Porosity and fluid overpressure profiles between the sea floor and 3-km depth are obtained from downhole measurement analysis (2% of the data points chosen randomly are here represented for the readability of the graph), and mud weight data. Both the porosity and the pressure data indicate the presence of three compartments between the sea floor and 3-km depth. The highly pressured compartments corresponds to an under-compacted compartment.

along fault planes, (2) the seismic anomalies associated with the growth faults, (3) the mechanical weakness of the fault zones, and (4) the fact that growth faults can sustain some fluid pressure differential between different pressured compartments. We draw below some concepts, which could explain these observations and which are

based on a poro-plastic rheology (for viscously deformable sediments see [22–24]).

From the observations described in the previous sections, growth faults act as preferential pathways that bring fluids (including in the present case hydrocarbons) repeatedly to the upper hydrostatic section of the sedimentary ba-

sin. To explain this episodicity of upward migration of fluids, the concept of a steady Darcean flow does not seem entirely appropriate. Formulation of flow in a poro-plastic deformable matrix [17] leads to some propagating wave-like flow solution along a conduit like a fault. These solutions correspond to porosity bumps or constrictions propagating upward like waves. These bumps or constrictions are accompanied by a pore fluid pressure dipole that is composed by a pair of positive and negative pressure changes. In granular porous media, the flux of fluids is strongly controlled by the pore fluid pressure below. Therefore, the persistence of high fluid pressure in deep compartments below the salt seals and connected to the roots of the growing faults by the presence of salt welds favors episodic expansion of the growing faults and can lead to the upward migration of these flow instabilities. The fault plane can be flexibly opened or closed in response to fluid pressure change in the deep compartments forming the fluid sources at depth and the ‘kitchen’ for hydrocarbon maturation. These pulses of pore fluid pressure, termed solitary waves [17], represent at the same time a fluid pressure dipole and a high fluid content pocket, both propagating upward at the same speed and generating a strong increase of permeability during its ascent along the fault plane.

We consider here travelling wave solutions to the problem of saturated flow of water through a uniform porous gouge filling a vertical fault plane. In a 1-D model, the set of equations describing the propagation of these pulses are:

$$\frac{\partial u}{\partial z} + \rho_f \frac{\partial \phi}{\partial t} = 0 \quad (2)$$

$$u = -\frac{k}{\eta_f} \left(\frac{\partial p}{\partial z} - \rho_f g \right) \quad (3)$$

$$k \equiv k_0 F(\sigma_{\text{eff}}) = k_0 \exp(-\sigma_{\text{eff}}/\sigma^*) \quad (4)$$

$$\phi \equiv \phi_0 G(\sigma_{\text{eff}}) = \phi_0 (1 - \beta \sigma_{\text{eff}}) \quad (5)$$

where u is the Darcy’s velocity (in m s^{-1}), t is time (in s), z is the depth (in m) from the top of the growing fault (assumed to be vertical here), ϕ is the porosity, g is the gravity acceleration, and ρ_f . Eq. 2 is the continuity equation, Eq. 3 represents the Darcy’s law, and Eqs. 4 and 5 represent constitutive relationships for the permeability and the porosity, which are both related to the effective stress as shown in Section 2, σ_{eff} is defined by $(\sigma - p)$, where σ is the confining stress (approximated here by the lithostatic stress) and p is the pore fluid pressure. This yields,

$$p = \sigma - \sigma_{\text{eff}} \quad (6)$$

$$\sigma = \int_0^z \rho g dz' \quad (7)$$

$$\rho = (1 - \phi)\rho_g + \phi\rho_f \quad (8)$$

where $\rho(z)$ is the bulk density of the sediment at depth z and ρ_g is the density of the grains. As σ is constant at a given depth during the passage of the pore fluid pressure disturbance, this yields the following equality,

$$\frac{\partial p}{\partial z} - \rho_f g = -\frac{\partial \sigma_{\text{eff}}}{\partial z} + (1 - \phi)(\rho_g - \rho_f)g \quad (9)$$

Combining Eqs. 2–5 and 9 yields a differential equation:

$$\frac{\partial}{\partial z} \left[\frac{k_0 F}{\phi_0 \eta_f \rho_f} \left(\frac{\partial \sigma_{\text{eff}}}{\partial z} - (1 - \phi)g(\rho_g - \rho_f) \right) \right] - \frac{\partial G}{\partial t} = 0 \quad (10)$$

in which the effective stress is the state variable. Indeed, F and G in Eq. 10 are explicit functions of the effective stress according to Eqs. 4 and 5, respectively. J. Rice [17] showed that wave-like solutions of Eq. 10 exist when F decreases with the effective stress faster than G. From Eqs. 4 and 5, this is presently the case. Actually this seems a quite general rule in porous materials as the permeability is usually a power-law of the porosity. These wave-like solutions take the form of upward propagating surges in pore fluid pressure

(or equivalently to a decrease in effective stress) due to a sudden increase of the pore pressure at the root of the growing fault. We can look for a solution on the form $\sigma_{\text{eff}} = f(z - ct)$ where c is the wave velocity. We assume from now that the decrease of the effective stress inside the heart of the disturbance reaches zero, which leads to fluidization of the gouge during the propagation of the solitary wave. We note, σ_0 the initial value of the effective stress inside the growing fault prior the arrival of the fluid pressure disturbance ($\sigma_0 \approx 5 \pm 3$ MPa inside the Red Fault system).

To find an expression for the speed of the solitary wave, we can replace $\partial/\partial t$ by $-c\partial/\partial z$, and integrate the partial differential equation (Eq. 10) in z from a position well ahead from the front of the disturbance to one at a general state σ_0 (σ_0 corresponding to the effective stress shock responsible for the solitary wave formation) [17]. This yields:

$$c \approx \left(\frac{1 - \phi_0}{\phi_0} \right) \frac{g k_0 (\rho_g - \rho_f)}{\eta_f \beta \sigma_0} \quad (11)$$

During the passage of a solitary wave there is a transient decrease of the effective stress. Thus the appropriate β entering into Eq. 11 would be that for elastic swelling from a pre-consolidation state, which is $\sim 1 \times 10^{-8}$ /Pa (see Fig. 5b). In addition, we use the following set of parameters $k_0 = 600$ mD (Fig. 4), $\phi_0 = 0.30$ (typical porosity of the fault gouge [13]), $\rho_g = 2650$ kg m $^{-3}$, $\rho_f = 800$ kg m $^{-3}$ (for a super-critical gas/oil mixture), $g = 9.81$ m s $^{-2}$, $\sigma_0 = 5$ MPa (maximum effective stress shock possible in the Red Fault), and $\eta_f = 10^{-4}$ Pa s. This yields $c = 160$ km/yr (we obtain $c = 16$ km yr $^{-1}$ with $\eta_f = 10^{-3}$ Pa s). If σ_0 is smaller (according to Fig. 4, $\sigma_0 < 2$ MPa), the velocity of the solitary wave is even higher. A decrease of two orders of magnitude of the permeability of the fractured shale (e.g. taking $k_0 = 1$ mD, $\sigma_0 = 1$ MPa, $\eta_f = 10^{-4}$ Pa s) yields $c = 1.3$ km yr $^{-1}$, which is still a substantial fluid transfer velocity compatible with the geochemical measurements presented in [20].

Fluids migration along the Red Fault system is strongly controlled by the pore fluid pressure existing at depths of 5–6 km, in highly pressured

compartments connected to this fault system. In particular, persistence of high fluid pressure in these compartments is a favorable condition to the episodic surges of pore pressure that propagates upward along the fault zone in a wave-like manner. These solitary waves are inevitably accompanied by dilatancy of the fault plane and probably by fluidization/fracturation of the gouge material (as the pore fluid pressure is already close to the minimum confining stress in the fault plane). Such dilatancy and fluidization phenomena are likely to be associated to the seismic anomalies observed by Anderson et al. [10] along the Red Fault system. Furthermore, as solitary waves propagate with a high velocity (> 1 km/yr), they would be associated with a burst of hot fluids moving up along the Red Fault system. This could explain partly the 10°C today-temperature anomaly reported along the Red Fault system and the 55°C past-temperature anomaly recorded by geochemical indicators in the same fault [8]. The velocity of the solitary wave can be so high that the surge of pore pressure could be roughly at the same temperature than initiated at the root of the growing fault. A pulse of instantaneous temperature of 125°C is inferred by Losh et al. [8] from geochemical consideration at a depth below 2 km in the Red Fault system. Such a temperature is characteristic of a depth of 5 km inside the basin, roughly the depth of the root of the Red Fault system. This observation is in agreement with the rapid upsurge of a fluid pressure pulse along the fault plane.

Another set of data suggests that, in the SEI area, a huge amount of hydrocarbons ascended rapidly to the shallow sand reservoirs from ~ 6 km depth [6–8,19]. These hydrocarbons result from maturation of the organic matter in deep sub-lithostatic pressured compartments, but the process of upward migration was not clear. The theory of propagation of solitary waves in porous materials [25] implies that the propagation of these waves is concomitant with a potentially strong expansion of the preferential pathways of migration. Therefore, the previous difficulty is eliminated by supposing that pressured fluids ascended with simultaneous formation of a highly permeable porous conduit (~ 600 mD, Fig. 5a) in

the fault zone. As the velocity of propagation of solitary waves is relatively fast, the presence of growth faults in compartmentalized sedimentary basins would be capable of transporting fluids, including mixtures of hydrocarbons (oil and methane), at high velocities, easily satisfying the constraints imposed by organic geochemical measurements. The frequency of these solitons is probably such as they allow to evacuate the oil and gas produced at depth in order to maintain the pore fluid pressure to the hydrofracturation breakdown curve at the roots of the listric faults. Another question arises about how do solitary waves die out and supply fluid to sands along the fault zone in the upper part of the basin. The solitary waves move up as long as the gas pressure at the tip of the cracks is high enough to allow them to propagate upward. However if the capillary entry pressure of the gas into the sediment is exceeded (which is more likely the case in the upper part of the basin where the growing faults are immature), the gas (and oil) would prefer to move out of the fault into the sand formations. This leads naturally to the end of the wave.

Another point concerns the observed mechanical weakness of the growing faults. Hubbert and Rubey [26] and later Sibson [27] have first recognized the importance of pore fluid pressure as a key factor explaining the mechanical weakness of faults in sedimentary basins. The propagation of solitary waves along fault planes is associated with pore fluid fluctuations. As the pore fluid pressure is already close to the minimum confining stress, a small perturbation of the pore fluid pressure can easily lead to fluidization of the gouge material. Therefore, the propagation of solitary waves, accompanied by local fluidization of the gouge, would relax the deviatoric component of the stress along the fault plane. Furthermore, if the porosity of the gouge material cannot inflate enough to allow the inflow of the pressured fluids, during the propagation of the solitary wave, tensile cracks would form to increase transiently the permeability of the fault material. Cracks filled by hydrocarbons have been observed in the Red Fault system [7].

Finally, the last paradox to solve concerns the

existence of faults acting both as boundaries between pressured compartments and as vertical fluid migration conduits. This means that the fast propagation of solitary waves does not interact greatly with the surrounding compartments. Numerical modelling of propagation of solitary waves along a high-porosity conduit can explain this feature. Richardson et al. [25] showed that during the upward propagation of solitary waves along a high-porosity conduit viscously deformable, three distinct regions of fluid flow can be observed: a central fast flow in the porous conduit (the solitary wave itself), a circulating flow in the boundary, and a slow background flow. They showed that the circulating flow decouples the propagation of the solitary waves with the surrounding matrix.

4. Concluding statements

The Red Fault is an active growth fault system located in the SEI minibasin and produced in response to salt withdrawal at few km depth inside the basin. This fault forms a subvertical permeability barrier, which bounds laterally overpressured compartments. In addition there is sufficient evidence of very localized episodic fluid migration (oil/gas super-critical mixture and very saline water) along the Red Fault over very short time scales (\sim years). The fault exhibits high fluid pressure above hydrostatic and consequently low effective stress. The new feature described in this paper is the possibility of fluid transfer through the propagation of solitary waves along the main growth fault present in this basin at the time scale of the year. This rapid transfer mechanism is in agreement with the great number of geophysical and geochemical observations made in this basin. The source of fluids comes from poorly compacted and overpressured compartments at depth and maturation of the organic matter in source rocks below the salt sills. Consequently, we believe that the phenomenon of solitary wave propagation in active growing faults is a fundamental mechanism, which can help to understand the nature of upward fast migration of fluids along growing faults in compartmentalized sedimentary

basins. This mechanism has broad interdisciplinary implications to the hydrodynamics of sedimentary basins worldwide.

Acknowledgements

This work is supported by the GBRN at Cornell University and it represents a direct outgrowth of a grant by the gas Research Institute to L.M.C.III (GRI No. 5093-260-2689). Elf Aquitaine (D. Grauls and O. Brévar) is particularly thanked for a grant given to A.R. during his stay at Cornell University. We thank Pennzoil, Landmark Graphics, and all the companies members of the GBRN, which have contributed to provide data and support the GBRN. We thank P. Henry for very stimulating discussions, and J.R. Rice and J.A. Nunn for their constructive reviews of the manuscript. [RV]

References

- [1] W.H. Fertl, Abnormal Formation Pressure, Implications to Exploration, Drilling, and Production of Oil and Gas Resources, Elsevier, Amsterdam, 1976, 382 pp.
- [2] A. Revil, L.M. Cathles, J.D. Shosa, P.A. Pezard, F.D. deLarouzière, Capillary sealing in sedimentary basins: a clear field example, *Geophys. Res. Lett.* 25 (1998) 389–392.
- [3] P.J. Ortoleva, Basin compartmentation: definitions and mechanisms, in: P.J. Ortoleva (Ed.), *Basin Compartments and Seals*, Mem. Am. Ass. Petrol. Geol. 61, 1995, pp. 39–51.
- [4] J.D. Bredehoeft, Fault permeability near Yucca Mountain, *Water Resour. Res.*, 1997, pp. 2459–2463.
- [5] L.L. Alexander, P.B. Flemings, Geologic evolution of a Pliocene–Pleistocene salt withdrawal mini-basin: Eugene Island Block 330, offshore Louisiana, *Am. Assoc. Pet. Geol. Bull.* 79 (1995) 1737–1756.
- [6] D. Coelho, Three Dimensional Analysis of the Temperature Field in Block 330, South Eugene Island, Gulf of Mexico, Ph.D. Thesis, Cornell University, Ithaca, NY, 1997, 292 pp.
- [7] S. Losh, Oil migration in major growth fault: structural analysis of the pathfinder core, South Eugene Island Block 330, offshore Louisiana, *Am. Assoc. Pet. Geol. Bull.* 82 (1998) 1694–1710.
- [8] S. Losh, L. Eglinton, M. Schoell, J. Wood, Vertical and lateral fluid flow related to a large growth fault, South Eugene Island Block 330 Field, offshore Louisiana, *Am. Assoc. Pet. Geol. Bull.* 83 (1999) 244–276.
- [9] D.S. Holland, J.B. Leedy, D.R. Lammelin, Eugene Island Block 330 field – USA, offshore Louisiana, Compilers, Structural Traps; III, Tectonic fold and fault traps, in: E.A. Beaumont, N.H. Foster (Eds.), *American Association of Petroleum Geologists, Treatise of Petroleum Geology, Atlas of Oil and Gas Fields*, 1990, pp. 103–143.
- [10] R. Anderson, P. Flemings, S. Losh, J. Austin, R. Woodhams, Gulf of Mexico growth fault drilled, seen as oil, gas migration pathway, *Oil and Gas J.* 92 (1994) 97–103.
- [11] S. Roberts, J.A. Nunn, Episodic fluid expulsion from geopressed sediments, *Mar. Pet. Geol.* 12 (1995) 195–204.
- [12] S. Roberts, J.A. Nunn, L.M. Cathles, F.-D. Cipriani, Expulsion of abnormally pressured fluids along faults, *J. Geophys. Res.* 101 (1996) 28231–28252.
- [13] J.A. Nunn, Pore Pressure Dependent Fracture Permeability and Ductile Shear Deformation in Fault Zones: Implications for Cross Formational Fluid Flow, *Am. Assoc. Pet. Geol. Memoir*, in press.
- [14] B.S. Hart, P.B. Flemings, A. Deshpande, Porosity and pressure Role of compaction disequilibrium in the development of geopressesures in a Gulf Coast Pleistocene basin, *Geology* 23 (1995) 45–48.
- [15] J.A. Nunn, Buoyancy-driven propagation of isolated fluid-filled fractures: implications for fluid transport in Gulf of Mexico geopressed sediments, *J. Geophys. Res.* 101 (1996) 2963–2970.
- [16] P. Pesca, M.D. Zoback, Compressive and tensile failure of inclined well bores and determination of in situ stress and rock strength, *J. Geophys. Res.* 100 (1995) 12791–12811.
- [17] J.R. Rice, Fault stress states, pore pressure distribution, and the weakness of the San Andreas Fault, in: B. Evans and T.-F. Wong (Eds.), *Fault Mechanics and Transport Properties in Rocks*, Academic Press, San Diego, 1992, pp. 475–503.
- [18] D.A. Elliott, Hydrofracture Permeability Response and Maximum Previous Consolidation Stress Estimations for Faulted and Micro-Fractured Silty–Shales Taken from the Eugene Island Block 330 Field Pathfinder Well in the Gulf Coast of Mexico, M.Sc. Thesis, University of California, San Diego, 1999, 103 pp.
- [19] J.K. Whelan, M.C. Kennicutt, J.M. Brooks, D. Schmacher, L.B. Eglinton, Organic geochemical indications of dynamic fluid flow processes in petroleum basins, *Org. Geochem.* 22 (1994) 587–615.
- [20] J.K. Whelan, L. Eglinton, M.C. Kennicutt II, Y. Qian, Short-time-scale (year) variations of petroleum fluids from the U.S. Gulf Coast, *Geochim. Cosmochim. Acta* 65 (2001) 3529–3555.
- [21] A. Revil, Thermal conductivity of unconsolidated sediments with geophysical applications, *J. Geophys. Res.* 105 (2000) 16749–16768.
- [22] A. Brown, Evaluation of possible gas microseepage mechanisms, *Am. Assoc. Pet. Geol. Bull.* 84 (2000) 1775–1789.
- [23] M. Appold, J.A. Nunn, Solitary Waves as Agents of Primary Hydrocarbon Transport in the Gulf of Mexico Ba-

- sin, EOS Transactions, American Geophysical Union, 1999, 1032.
- [24] M. Appold, J.A. Nunn, Numerical models of petroleum migration via buoyancy-driven porosity waves in viscously deformable sediments, *Geofluids*, in press.
- [25] C.N. Richardson, J.R. Lister, D. McKenzie, Melt conduits in a viscous porous matrix, *J. Geophys. Res.* 101 (1986) 20423–20432.
- [26] M.K. Hubbert, W.W. Rubey, Mechanics of fluid filled porous solids and its implication to overthrust faulting. I. Role of fluid pressure in mechanics of overthrust faulting, *Geol. Soc. Am. Bull.* 70 (1959) 115–166.
- [27] R. Sibson, Conditions for fault-wave behaviour, in: R.J. Knipe, E.H. Rutter (Eds.), *Deformation Mechanisms, Rheology and Tectonics*, *Geol. Soc. Spec. Publ.* 54, 1990, pp. 15–28.